Characterization of a Weyl semimetal using a unique feature of surface plasmon polaritons

Kota Tsuchikawa*
Department of Physics, Faculty of Science, Tokyo University of Science, Tokyo 162-8601, Japan and Nanolectronics Research Institute (NeRI), National Institute of Advanced Industrial Science and Technology (AIST), Ibaraki 305-8568, Japan

Satoru Konabe†
Department of Chemical Science and Technology, Hosei University, Tokyo 184-8584, Japan
Research Institute for Science and Technology, Tokyo University of Science, Tokyo 125-8585, Japan
and Device Technology Research Institute, National Institute of Advanced Industrial Science and Technology (AIST), Ibaraki 305-8568, Japan

Takahiro Yamamoto
Department of Physics, Faculty of Science, Tokyo University of Science, Tokyo 162-8601, Japan

Shiro Kawabata
Device Technology Research Institute, National Institute of Advanced Industrial Science and Technology (AIST), Ibaraki 305-8568, Japan

(Received 17 March 2020; accepted 16 July 2020; published 30 July 2020)

We theoretically investigate the decay constant of surface plasmon polaritons in a Weyl semimetal and propose an experimental method for detecting Weyl semimetals. It is revealed that the surface plasmon polariton in a Weyl semimetal exhibits various characteristics depending on the plasmon wave vector. It can be a pure surface wave, a pseudosurface wave that couples with a bulk plasmon, or a generalized surface wave with complex decay constants. Such diverse surface plasmon characteristics are peculiar to Weyl semimetals that obey axion electrodynamics. The results suggest that the measurement of the decay length, the inverse of the decay constant, can be a powerful experimental probe for identifying Weyl semimetals.

DOI: 10.1103/PhysRevB.102.035443

I. INTRODUCTION

The Weyl fermion, which is a massless spin-1/2 particle satisfying the Weyl equation, was theoretically predicted in 1929 [1]. Its experimental verification has been a long-standing problem in the field of high-energy physics. In the field of condensed-matter physics, it has recently been predicted that low-energy elementary excitations (quasiparticles) in some kinds of topological materials can be regarded as Weyl fermions [2–7]. The experimental verification and synthesis of such materials, referred to as Weyl semimetals, has attracted attention [8–25]. Due to the nontrivial band topology [26–28] of Weyl semimetals that consist of a pair of Dirac dispersions (Fig. 1), it has been theoretically predicted that Weyl semimetals exhibit surface state effects by Fermi arc [29–33], anomalous transport phenomena [3,7,26,31,34–43], optical [16,44–53], electromagnetic [7,51,54–65], and density responses [66–69].

In particular, Weyl semimetals exhibit exotic electromagnetic effects because they are effectively described by Maxwell's equations with axion modifications [16,44,51,54,70]. Electromagnetic properties in a Weyl semimetal are derived from the effective action

$$S = \frac{e^2}{4\pi\hbar c}\int dtd\boldsymbol{r}\theta(\boldsymbol{r},t)\boldsymbol{E}\cdot\boldsymbol{B}, \tag{1}$$

where $\boldsymbol{E}$ ($\boldsymbol{B}$) is the electric (magnetic) field and $\theta(\boldsymbol{r},t)$ characterizes a topological property. For a time-reversal-breaking system, which is studied in the present paper, $\theta(\boldsymbol{r}) = 2\boldsymbol{b}\cdot\boldsymbol{r}$, where $\boldsymbol{b}$ is the wave vector that connects the two Weyl points in the reciprocal space, as shown in Fig. 1.

A wave vector $\boldsymbol{b}$ can be controlled by modifying material parameters. Indeed, once a Hamiltonian is given, $\boldsymbol{b}$ can be expressed as variables in the Hamiltonian. For example, the following expression of the magnitude of $\boldsymbol{b}$ has been given for the topological insulator superlattice [4]

$$|\boldsymbol{b}| = \frac{2}{d}\cos^{-1}\left(\frac{\Delta_S^2+\Delta_D^2-m^2}{2\Delta_S\Delta_D}\right), \tag{2}$$

where d is the multilayer period of the superlattice, Δ_S (Δ_D) is the hopping parameter, which describes tunneling between top and bottom surfaces within a given (neighboring) topological insulator layer(s), and m is the amplitude of the exchange spin splitting of the surface states induced by doped magnetic impurities. It is noted that Eq. (2) is valid only in a Weyl semimetal region that satisfies $-m+\Delta_S \leqslant \Delta_D \leqslant m+\Delta_S$

*Present address: Department of Physics, Graduate School of Science and Engineering, Tokyo Metropolitan University, Hachioji, Tokyo 192-0397, Japan.
†konabe@hosei.ac.jp

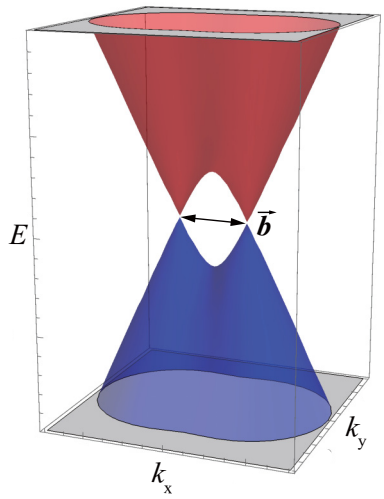

FIG. 1. Energy band of a Weyl semimetal with vector $\boldsymbol{b}$ that connects the Weyl points.

and $\Delta_D \geqslant m - \Delta_S$. A Weyl semimetallic state arising from the topological superlattice is expected to be realized in GeTe-Sb_2Te_3 superlattices [71].

In Ref. [51], Hofmann and Das Sarma theoretically showed a peculiar surface plasmon polariton (SPP) dispersion in Weyl semimetals, where the dispersion curve disappears in a certain wave-vector region. However, the details of the electromagnetic phenomena in the coexistence region are not fully understood. In this paper, we thus theoretically investigate the decay constant of the SPP in Weyl semimetals, which is the inverse of the decay length of SPPs into a bulk region. From the analysis of the decay constant, we elucidate the peculiar feature of the SPP in Weyl semimetals.

II. THEORY

In this section, we briefly review the theory of SPPs in Weyl semimetals [51]. For a Weyl semimetal under the conditions of neutral charge and zero current, the wave equation for electric field $\boldsymbol{E}$ (that for magnetic field $\boldsymbol{H}$ is not shown here) can be easily derived from the action (1) as

$$\nabla \times (\nabla \times \boldsymbol{E}) + \frac{1}{c^2}\frac{\partial^2}{\partial t^2}\boldsymbol{D} = 0, \tag{3}$$

where $\boldsymbol{D}$ is given as

$$\boldsymbol{D} = \varepsilon_1(\omega)\boldsymbol{E} + i\varepsilon_2(\omega)\hat{\boldsymbol{e}}_{\boldsymbol{b}} \times \boldsymbol{E}, \tag{4}$$

where $\hat{\boldsymbol{e}}_{\boldsymbol{b}} \equiv \boldsymbol{b}/|\boldsymbol{b}|$. For Eq. (4), we define the dielectric functions

$$\varepsilon_1(\omega) = \varepsilon_0\varepsilon_b\left(1 - \frac{\omega_p^2}{\omega^2}\right), \tag{5}$$

$$\varepsilon_2(\omega) = \varepsilon_0\varepsilon_b\frac{\omega_b^2}{\omega^2}, \tag{6}$$

where $\omega_p = \sqrt{\frac{4e^2}{3\pi\hbar v_F \varepsilon_b}}\frac{E_F}{\hbar}$ is the plasmon frequency of a Weyl semimetal [68], where v_F is the Fermi velocity and E_F is the Fermi energy, and $\omega_b \equiv 2e^2|\boldsymbol{b}|/\pi\hbar\varepsilon_b$. Throughout this paper,

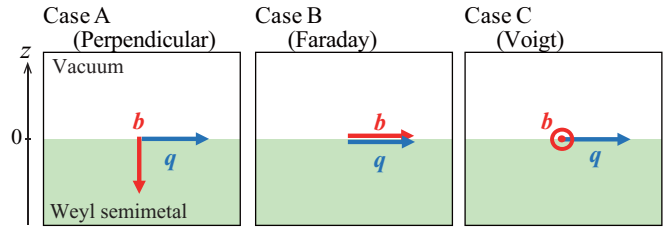

FIG. 2. Geometry of the interface between a vacuum and a Weyl semimetal. The Weyl semimetal is located in the negative half $z \leqslant 0$, and there is a vacuum in the positive half $z > 0$.

we adopt the following value for the static dielectric constant of a Weyl semimetal, $\varepsilon_b = 13$ for $Eu_2Ir_2O_7$ [16], which is a candidate Weyl semimetal.

It is apparent from Eq. (4) that the dielectric tensor has off-diagonal components ε_2 due to the chiral anomaly represented by the θ term. Therefore, a Weyl semimetal may exhibit an anisotropic response to an electromagnetic field, similar to other materials doing so in the presence of an external magnetic field.

For solving the wave equation [Eq. (3)], we assume the following geometry: A Weyl semimetal is located in the negative half $z \leqslant 0$, and there is a vacuum in the positive half $z > 0$ (see Fig. 2). The wave equation is solved assuming the plane wave

$$\boldsymbol{E} = \boldsymbol{E}_0 e^{iq_x x + iq_y y} e^{-\kappa|z|} e^{-i\omega t}, \tag{7}$$

where $q_x(q_y)$ and ω are, respectively, the wave vector and frequency of a plasmon at the interface of the Weyl semimetal and the vacuum (xy plane), and κ is the decay constant used to express the inverse of the decay length for the evanescent wave along the z direction.

For considering the SPP, the following three configurations are possible depending on the relative direction between the wave vector $\boldsymbol{q}$ of the plasmon and the vector $\boldsymbol{b}$ (see also Fig. 2) [51].

(i) Case A (Perpendicular configuration):
$\boldsymbol{q} \parallel xy$ plane and $\boldsymbol{b} \parallel z$ axis,
(ii) Case B (Faraday configuration):
$\boldsymbol{q} \parallel xy$ plane and $\boldsymbol{b} \parallel xy$ plane ($\boldsymbol{q} \parallel \boldsymbol{b}$),
(iii) Case C (Voigt configuration):
$\boldsymbol{q} \parallel xy$ plane and $\boldsymbol{b} \parallel xy$ plane ($\boldsymbol{q} \perp \boldsymbol{b}$).

We set $\boldsymbol{q} = (q, 0, 0)$ hereafter. The SPP dispersion is determined by enforcing the continuity of the parallel components of $\boldsymbol{E}$ and $\boldsymbol{B}$ and that of the perpendicular components of $\boldsymbol{D}$ and $\boldsymbol{B}$.

For case A, the boundary condition provides the following equation

$$[\kappa_+(q,\omega) - \kappa_-(q,\omega)]M_\perp(q,\omega,\kappa_+,\kappa_-) = 0, \tag{8}$$

where

$$M_\perp(q,\omega,\kappa_+,\kappa_-) = [\kappa_+\kappa_- + \kappa_0(\kappa_+ + \kappa_-) + q^2]\,q^2 + \frac{\varepsilon_1^2\omega^2 q^2}{c^2} + \varepsilon_1\left[\kappa_0^2(\kappa_+^2 + \kappa_+\kappa_- + \kappa_-^2 - q^2)\right.$$

$$+\kappa_0(\kappa_+ + \kappa_-)\left(\kappa_+\kappa_- - \frac{\omega^2}{c^2}\right) - \frac{(\kappa_+\kappa_- + 2q^2)\omega^2}{c^2}\Bigg]. \quad (9)$$

Here, $\kappa_0^2 = q^2 - (\omega/c)^2$ for the vacuum and

$$\kappa_\pm^2(q,\omega) = q^2 - \frac{\varepsilon_1\omega^2}{c^2} \pm \sqrt{\frac{\varepsilon_2^2\omega^2}{\varepsilon_1 c^2}\left(\frac{\varepsilon_1\omega^2}{c^2} - q^2\right)}, \quad (10)$$

for the Weyl semimetal.

For case B with $\boldsymbol{q} = (q, 0, 0)$ and $\boldsymbol{b} = (b, 0, 0)$, the boundary condition provides the following equation

$$[\kappa_+(q,\omega) - \kappa_-(q,\omega)]M_\parallel(q,\omega,\kappa_+,\kappa_-) = 0, \quad (11)$$

where

$$M_\parallel(q,\omega,\kappa_+,\kappa_-) = \kappa_+\kappa_-(\kappa_+ + \kappa_-) + \kappa_0(\kappa_+\kappa_- + q^2) + \frac{\kappa_0\varepsilon_1\omega^2}{c^2} + \varepsilon_1\kappa_0\left[\kappa_+^2 + \kappa_+\kappa_- + \kappa_-^2 + \kappa_0(\kappa_+ + \kappa_-) - q^2 - \frac{\varepsilon_1\omega^2}{c^2}\right]. \quad (12)$$

Here,

$$\kappa_\pm^2(q,\omega) = q^2 - \frac{\varepsilon_1\omega^2}{c^2} + \frac{\varepsilon_2^2\omega^2}{2\varepsilon_1 c^2} \pm \sqrt{\frac{\varepsilon_2^2\omega^2}{\varepsilon_1 c^2}\left(\frac{\varepsilon_2^2\omega^2}{4\varepsilon_1 c^2} + q^2\right)}. \quad (13)$$

Because of the off-diagonal components ε_2 in the dielectric function, the Weyl semimetal region can support two decay constants, namely κ_+ and κ_-. Accordingly, the electric field may become

$$\boldsymbol{E} = (\boldsymbol{E}_+ e^{-\kappa_+|z|} + \boldsymbol{E}_- e^{-\kappa_-|z|})e^{i(qx-\omega t)}. \quad (14)$$

The SPP dispersion relation is derived from $M_\perp(q,\omega) = 0$ ($M_\parallel(q,\omega) = 0$) for $\kappa_+ \neq \kappa_-$. The associated decay constant is calculated by inserting the dispersion into Eq. (10) [Eq. (13)]. In addition, the bulk plasmon is obtained from $\kappa_+(q,\omega) = 0$ or $\kappa_-(q,\omega) = 0$.

For case C, it has been shown that the SPP dispersion is nonreciprocal [51]; the dispersion relation depends on the sign of $\boldsymbol{q}$, as commonly observed for normal metals in the presence of a magnetic field [72]. In addition, surface plasmons in this configuration couple with collective modes of Fermi arc states, called as Fermi arc plasmons [69,73,74]. These studies found a gapped dispersion and a gapless linear dispersion with a chiral character. On the other hand, effects by Fermi arc states on SPPs are studied in Ref. [75]. Below, we investigate SPPs for case A and case B, where Fermi arc states are not involved [69,73–75], to focus on the peculiarity due to the chiral anomaly.

III. RESULTS AND DISCUSSION

It is known that for both case A and case B, there exists a wave-vector region where the SPP dispersion disappears [51]; such phenomena were first found for SPPs in the presence of an external magnetic field [72]. For understanding such a peculiar plasmon more deeply, in this paper, we investigate the associated decay constants in addition to the dispersions.

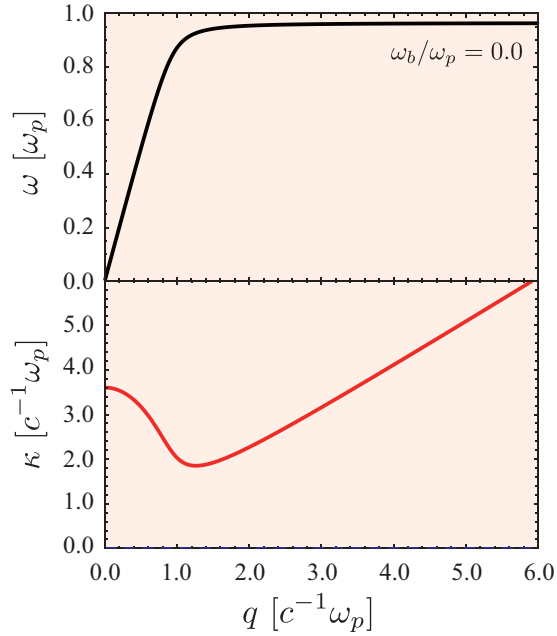

FIG. 3. Surface plasmon dispersion (upper panel) and decay constant (lower panel) for a Dirac semimetal (i.e., $\omega_b/\omega_p = 0$).

Before considering the case of a Weyl semimetal with a finite ω_b, we show the result for a Dirac semimetal, which is obtained using Eqs. (8) and (11) with $\omega_b = 0$. The dispersion and decay constant are shown in the upper and lower panels of Fig. 3, respectively. The frequency of the surface plasmon approaches the characteristic surface plasmon frequency $\omega = \omega_p\sqrt{\varepsilon_b/(\varepsilon_b+1)}$ in a short wavelength limit. On the other hand, the minimum of the decay constant is given by $\kappa = 2\omega_p\varepsilon_b/c(\varepsilon_b+1)$ at the wave vector of $q = \omega_p\sqrt{2\varepsilon_b(\varepsilon_b-1)}/c(\varepsilon_b+1)$. Thus, the dispersion and decay constant of a Dirac semimetal are similar to those of a normal metal with a Drude dielectric function.

Next, we see the dispersion relations and decay constants for SPPs for a Weyl semimetal with $\omega_b/\omega_p = 0.2,\ 0.5,\ 1.0$. The SPP dispersions (decay constants) are plotted in the upper (lower) panels of Figs. 4 and 5 for case A and case B, respectively.

Regarding the dispersion relations, the ω_b dependence is similar for case A and case B [51]. Indeed, as ω_b increases, the frequency of the bulk plasmon becomes lower than ω_p. As a consequence, the SPP is pushed down and overlaps the bulk plasmon in the wavevector region (purple regions in Figs. 4 and 5). In this region, the pure SPP disappears, leaving a gap; such a plasmon is called a pseudo-SPP [72]. The pseudo-SPP was first investigated for a magnetoplasmon in Ref. [72] and then for a Weyl semimetal in Ref. [51]. The ω_b dependence of the gap is shown in Fig. 6; the upper panels plot the gap in the frequency and the lower panels plot that in the wave vector.

We now examine the ω_b dependence of the decay constant for a Weyl semimetal. Despite the similarity of the peculiar

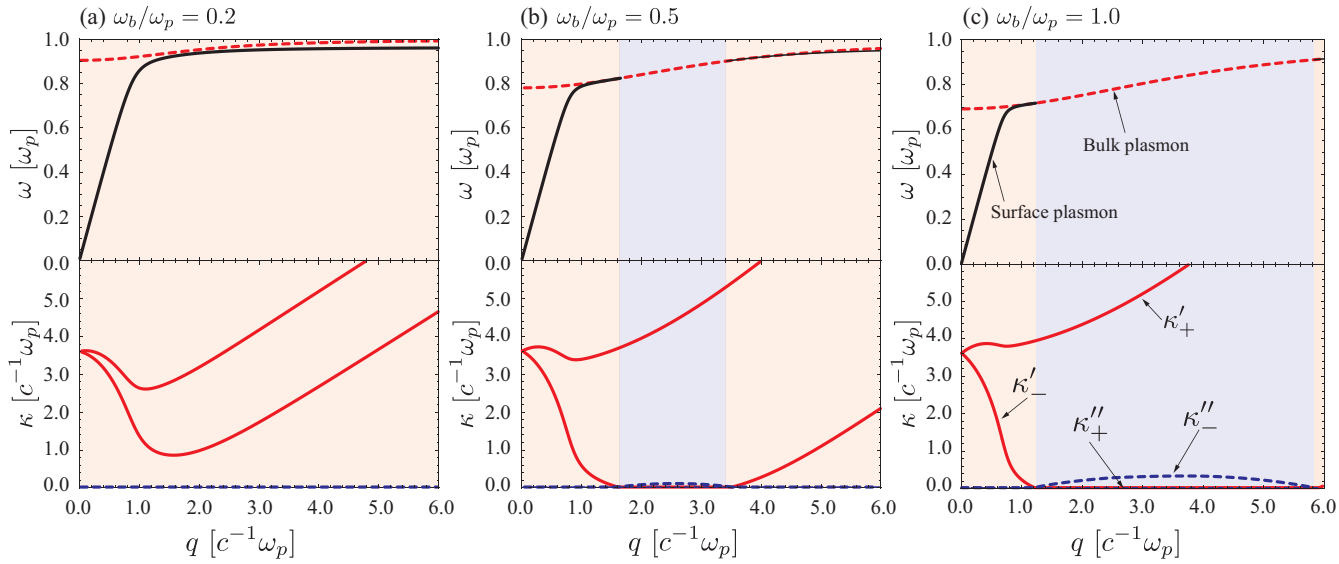

FIG. 4. Dispersion relations (upper panels) and decay constants (lower panels) of case A for (a) $\omega_b/\omega_p = 0.2$, (b) $\omega_b/\omega_p = 0.5$, and (c) $\omega_b/\omega_p = 1.0$. In the upper panels, the black curve represents the SPP dispersion and the red dashed curve represents the bulk propagating plasmon. In the lower panels, the red (blue dashed) curve represents the real (imaginary) part of the decay constant, i.e., $\kappa'_\pm$ ($\kappa''_\pm$). The orange and purple background regions correspond to the pure SPP and the pseudo-SPP, respectively.

feature observed for the plasmon dispersion between case A and case B [51], we found that the decay constant behaves differently for the two cases as shown below.

The lower panels of Fig. 4 show the ω_b dependence of decay constants for case A. For $\omega_b/\omega_p = 0.2$, shown in Fig. 4(a), the decay constants only have real parts with two different values. Therefore, the SPP for such a small ω_b is localized near the boundary as a pure surface wave (colored orange), which is similar to that for the Dirac semimetal shown in Fig. 3. For $\omega_b/\omega_p = 0.5$, shown in Fig. 4(b), one of the decay constants, say κ_+, is still real and the other, κ_-, becomes pure imaginary in the wave-vector region (colored purple). The electric field in the region is given by the superposition of the surface wave and the bulk propagating wave:

$$\boldsymbol{E} = (\boldsymbol{E}_+ e^{-\kappa'_+|z|} + \boldsymbol{E}_- e^{-i\kappa''_-|z|})\, e^{i(qx-\omega t)}, \tag{15}$$

where $\kappa'_\pm$ and $\kappa''_\pm$ are the real and imaginary p art of $\kappa_\pm$, respectively. An increase in ω_b extends the gap region, as clearly shown in Fig. 4(c). From the above analysis, a SPP of a Weyl semimetal for case A (the perpendicular configuration) can be

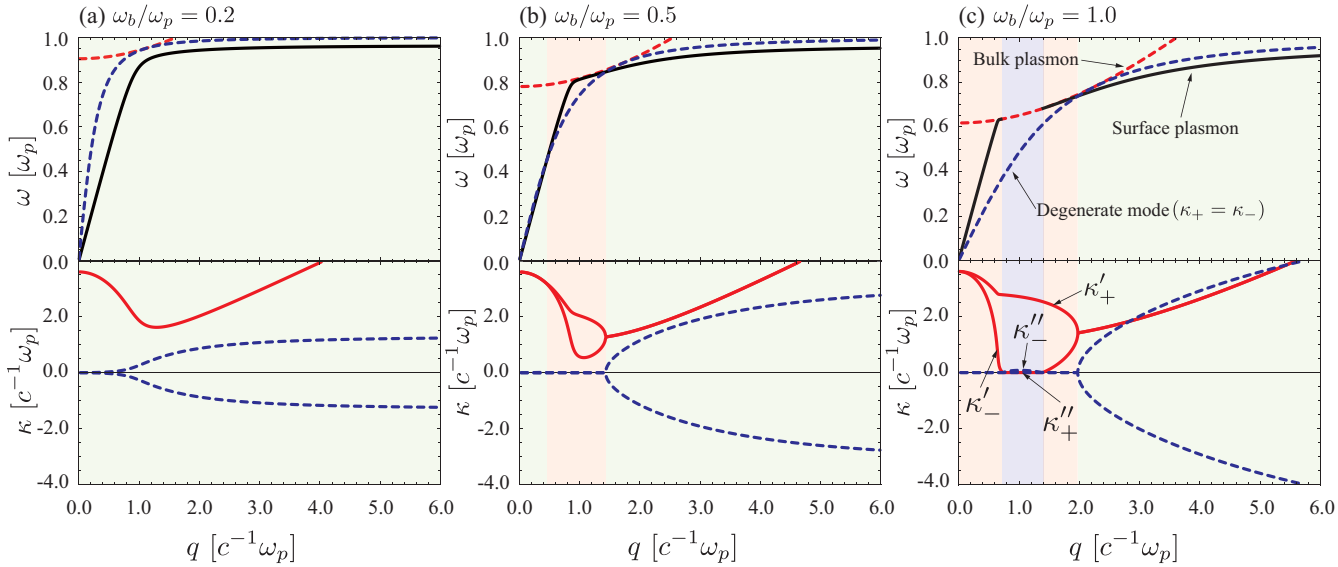

FIG. 5. Dispersion relations (upper panels) and decay constants (lower panels) of case B for (a) $\omega_b/\omega_p = 0.2$, (b) $\omega_b/\omega_p = 0.5$, and (c) $\omega_b/\omega_p = 1.0$. In the upper panels, the black curve represents the SPP dispersion and the red dashed curve represents the bulk propagating plasmon. In addition to the real modes, we plot the degenerate mode as the blue dashed curves. In the lower panels, the red (blue dashed) curve represents the real (imaginary) part of the decay constant, i.e., $\kappa'_\pm$ ($\kappa''_\pm$). The orange, purple, and green background regions correspond to the pure SPP, pseudo-SPP, and generalized SPP, respectively.

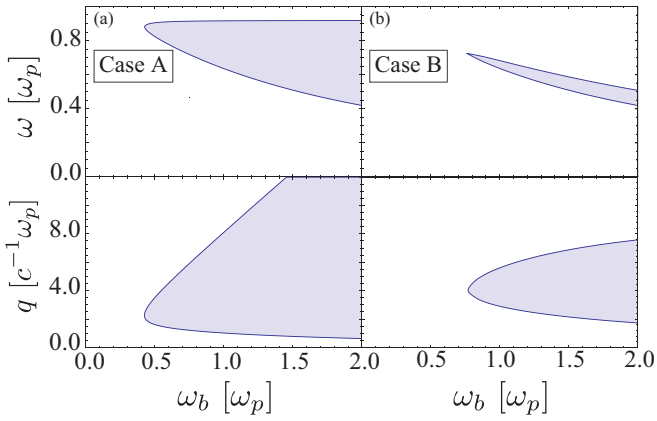

FIG. 6. Gap region of the pseudo-SPP for (a) case A and (b) case B. The upper (lower) panels show a gap in the frequency (wave vector).

a pure surface wave or a pseudosurface wave depending on the wave vector.

The lower panels of Fig. 5 show the ω_b dependence of decay constants for case B. For $\omega_b/\omega_p = 0.2$, shown in Fig. 5(a), the decay constants κ_+ and κ_- are complex conjugates of each other (green region). Therefore, even for such a small ω_b, for which the SPP behaves as a pure surface wave for case A, the SPP is different from those for normal metals and for the configuration of case A of a Weyl semimetal; actually it is not a pure surface wave but a damped oscillating wave:

$$\boldsymbol{E} = [\boldsymbol{E}_1 \cos(\kappa''|z|) + \boldsymbol{E}_2 \sin(\kappa''|z|)]\, e^{-\kappa'|z|} e^{i(qx-\omega t)}, \quad (16)$$

where we denote $\kappa_\pm = \kappa' \pm i\kappa''$, $\boldsymbol{E}_1 \equiv \boldsymbol{E}_+ + \boldsymbol{E}_-$, and $\boldsymbol{E}_2 \equiv i(\boldsymbol{E}_+ - \boldsymbol{E}_-)$. This type of the SPP is called a generalized SPP in Ref. [72]. For $\omega_b/\omega_p = 0.5$, shown in Fig. 5(b), a pure SPP appears (orange region). With a further increase of ω_b to $\omega_b/\omega_p = 1.0$, shown in Fig. 5(c), the region of the generalized SPP disappears at long wavelengths and the pseudo-SPP appears within the region of the pure surface wave. Therefore, SPPs of a Weyl semimetal for case B (the Faraday configuration) can be a pure surface wave, a pseudo-surface wave, or a generalized surface wave depending on the wave vector. The surface mode for case B thus exhibits more diverse and richer characteristics compared with that for case A. To see the difference more clearly, in Fig. 7, we plot the decay constants for case A and case B as a function of $\omega_b/\omega_\mathrm{p}$ for the fixed momentum of $cq/\omega_\mathrm{p} = 1.8$ and $cq/\omega_\mathrm{p} = 1.0$, respectively.

We now consider the origin of the different behaviors in the decay constants for case A and case B. The decay constants in Eqs. (10) and (13) have a structure of

$$\kappa_\pm^2(q,\omega) = A(q,\omega) \pm \sqrt{D(q,\omega)}. \quad (17)$$

For $D > 0$, κ_+ and κ_- become real with different values, and for $D < 0$, κ_+ and κ_- become complex conjugates of each other. For case A, the condition of $D > 0$ is equivalent to

$$0 < \omega < \omega_p \text{ or } \omega > \omega_p \sqrt{1 + \frac{1}{\varepsilon_0 \varepsilon_b}\left(\frac{cq}{\omega_p}\right)^2}. \quad (18)$$

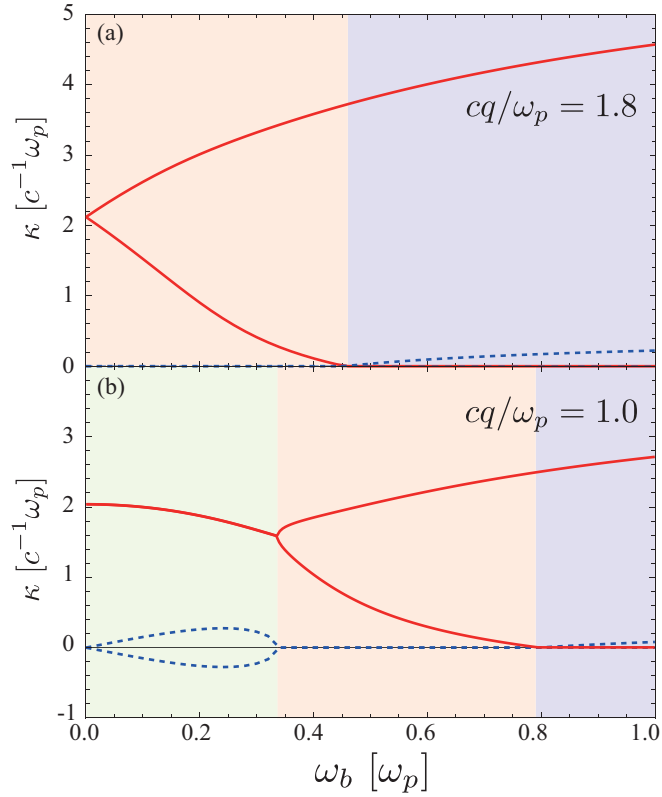

FIG. 7. Decay constants of (a) case A at $cq/\omega_\mathrm{p} = 1.8$ and (b) case B at $cq/\omega_\mathrm{p} = 1.0$ as a function of $\omega_b/\omega_\mathrm{p}$. The red (blue dashed) curve represents the real (imaginary) part of the decay constant, i.e., $\kappa'_\pm$ ($\kappa''_\pm$).The orange, purple, and green background regions correspond to the pure SPP, pseudo-SPP, and generalized SPP, respectively.

Therefore, the SPP dispersion derived from $M_\perp(q,\omega) = 0$ always satisfies the condition of $D > 0$. Consequently, only the pure SPP and the pseudo-SPP appear for case A.

For case B, there is a region of (q,ω) where the condition of $D < 0$ is satisfied. Indeed, the curve $D = 0$, which can be written as

$$\omega = \omega_p \left[1 + \frac{\varepsilon_0 \varepsilon_b \omega_b^2}{4}\left(\frac{\omega_p}{cq}\right)^2\right]^{-1/2}, \quad (19)$$

spans the dispersion relation derived from $M_\parallel(q,\omega,\kappa_+,\kappa_-) = 0$ (see the blue dashed curve representing $D = 0$ in the lower panel of Fig. 5). As a result, when the SPP dispersion is located above (below) the curve represented by $D = 0$, it becomes a pure (generalized) surface wave.

We note that $D = 0$ is equivalent to the relation $\kappa_+ - \kappa_- = 0$. Therefore, the points of (q,ω) satisfying $D = 0$ also meet the boundary condition, i.e., the relation in Eq. (11). This is called a degenerate mode, which was extensively studied for a magnetoplasmon a few decades ago [76–79]. For a degenerate mode, the solution [Eq. (14)] of the wave equation becomes

$$\begin{aligned}\boldsymbol{E} &= (\boldsymbol{E}_+ e^{-\kappa|z|} + \boldsymbol{E}_- e^{-\kappa|z|}) e^{i(qx-\omega t)} \\ &= \boldsymbol{E}' e^{-\kappa|z|} e^{i(qx-\omega t)},\end{aligned} \quad (20)$$

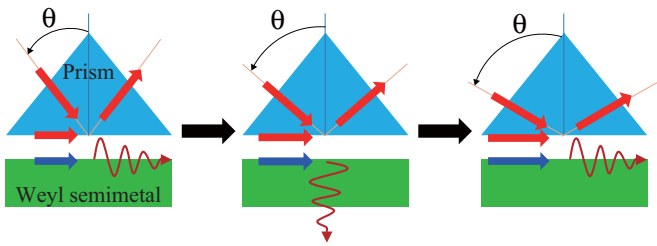

FIG. 8. Experimental setup that can be used to observe the bulk-penetrating SPP. The red arrow indicates the light direction and the blue arrow indicates the plasmon direction. The wavy line indicates the SPP. The light angle increases from left to right. At a certain angle θ of the light direction (center panel), the SPP penetrates the bulk region.

with $\boldsymbol{E}' \equiv \boldsymbol{E}_+ + \boldsymbol{E}_-$, where $\kappa_+ = \kappa_- = \kappa$. It has been shown that $\boldsymbol{E}'$ that satisfies the boundary condition should be zero, resulting in a trivial solution [79]. Therefore, there is no electromagnetic field corresponding to the degenerate mode, which means that the degenerate mode is not a physical mode but just expresses the line that divides the SPP into pure and generalized surface waves. At the points (q, ω) where both $\kappa_+ - \kappa_- = 0$ and $M_\parallel(q, \omega, \kappa_+, \kappa_-) = 0$ are satisfied, we thus adopt a different form of the solution for the wave equation since the plane wave solution does not exist. The following form of the wave can be used to solve the wave equation [80–82]

$$\boldsymbol{E} = (\boldsymbol{A} + \boldsymbol{B}|z|)e^{-\kappa|z|}e^{i(qx-\omega t)}, \tag{21}$$

with some vectors $\boldsymbol{A}$ and $\boldsymbol{B}$. The dispersion for such a wave is obtained from $M_\parallel(q, \omega, \kappa_+, \kappa_-) = 0$ with $\kappa_\pm$ replaced by κ.

Having elucidated the peculiar behavior of the decay constants of the SPP in a Weyl semimetal, we now propose an experimental setup for identifying Weyl semimetals by measuring the SPP. As shown above, for some wave-vector region, we have the superposition of the surface wave and bulk propagating wave as a pseudosurface wave, which leaks into the bulk region. Therefore, if the leak due to the pseudosurface wave is observed, we can identify a material as a Weyl semimetal.

We estimated the relevant values for measuring the leak for the configuration of case A. When we use $\omega_b/\omega_p = 0.5$ and $\varepsilon_b = 13$, the frequency where the leak occurs due to the pseudosurface wave is in the range of $0.7 \leqslant \omega/\omega_p \leqslant 0.9$, obtained from the upper panel of Fig. 6(a). This corresponds to $5.8 \leqslant \omega \leqslant 7.5$ THz for $E_F = 10$ meV and $58 \leqslant \omega \leqslant 75$ THz for $E_F = 100$ meV. In this region, the decay length $\xi \equiv 1/\kappa_+$ is estimated as $7.2 \leqslant \xi \leqslant 10$ μm for $E_F = 10$ meV and $0.72 \leqslant \xi \leqslant 1.0$ μm for $E_F = 100$ meV. Therefore, if the leak is measured for a sample with a thickness larger than ξ, we can identify the sample as a Weyl semimetal since the leak originated from the pseudosurface wave.

The experimental setup for detecting the leak is shown in Fig. 8. With the usual setup of the Otto configuration, the light is irradiated onto a prism (triangle in Fig. 8). Up to a certain angle of the irradiation light, only the evanescent wave exists in the Weyl semimetal. With increasing angle, the SPP becomes coupled to the bulk plasmon at a certain range of the wave vector, resulting in penetration into the bulk region. Therefore, at a certain range of the incident angle, we can observe light from the bottom of the prism, which indicates that the material placed under the prism is a Weyl semimetal. In addition, the measurement of the reflection spectra provides further information on the characteristics of the SPP. We note that the Kretschmann configuration as well as the Otto configuration can be applied to detect the above phenomenon, especially for the latter measurement.

IV. SUMMARY

In the present work, we theoretically investigated the SPP of a Weyl semimetal for two different geometrical configurations (perpendicular and Faraday) of interface, focusing on the decay constant. Even though the dispersion relation is similar for both configurations as found in the previous studied, the decay constant behaves completely different and exhibits diverse characteristics. Indeed, from the analysis of the decay constant, we found that the SPP of a Weyl semimetal for the perpendicular configuration (case A) becomes a pure surface wave or a pseudosurface wave depending on the wave vector, while for the Faraday configuration (case B), it becomes a pure surface wave, a pseudosurface wave, or a generalized surface wave. The diverse behavior of SPPs is one of essential features to understand a peculiar behavior due to the chiral anomaly of Weyl semimetals. We then proposed an experimental method and a setup for probing a Weyl semimetal by measuring such unusual surface modes, which are a unique feature of Weyl semimetals. The unusual surface modes, such as the generalized mode, in a Weyl semimetal can be used as a frequency or wave-number filter for plasmonic circuits and crystals.

ACKNOWLEDGMENTS

We acknowledge T. Tamaya for useful discussions. This work was partially supported by the JST Nanotech Carrier-up Alliance (CUPAL), a JSPS KAKENHI Grant No. 15H03523, a JSPS KAKENHI Grant No. 16H06331, a JST CREST Grant No. JPMJCR14F1, and a JST CREST Grant No. JPMJCR18I5.

[1] H. Weyl, Z. Phys. **56**, 330 (1929).
[2] S. Murakami, New J. Phys. **9**, 356 (2007).
[3] X. Wan, A. M. Turner, A. Vishwanath, and S. Y. Savrasov, Phys. Rev. B **83**, 205101 (2011).
[4] A. A. Burkov and L. Balents, Phys. Rev. Lett. **107**, 127205 (2011).
[5] G. B. Halász and L. Balents, Phys. Rev. B **85**, 035103 (2012).

[6] Z. Wang, Y. Sun, X.-Q. Chen, C. Franchini, G. Xu, H. Weng, X. Dai, and Z. Fang, Phys. Rev. B **85**, 195320 (2012).

[7] P. Hosur and X. Qi, C. R. Phys. **14**, 857 (2013).

[8] G. Xu, H. Weng, Z. Wang, X. Dai, and Z. Fang, Phys. Rev. Lett. **107**, 186806 (2011).

[9] S. M. Huang, S. Y. Xu, I. Belopolski, and C. C. Lee, Nat. Commun. **6**, 7373 (2015).

[10] B. Q. Lv, H. M. Weng, B. B. Fu, X. P. Wang, H. Miao, J. Ma, P. Richard, X. C. Huang, L. X. Zhao, G. F. Chen, Z. Fang, X. Dai, T. Qian, and H. Ding, Phys. Rev. X **5**, 031013 (2015).

[11] S. Y. Xu, I. Belopolski, N. Alidoust, M. Neupane, and G. Bian, Science **349**, 613 (2015).

[12] B. Q. Lv, N. Xu, H. M. Weng, J. Z. Ma, P. Richard, X. C. Huang, L. X. Zhao, G. F. Chen, C. E. Matt, F. Bisti, V. N. Strocov, J. Mesot, Z. Fang, X. Dai, T. Qian, M. Shi, and H. Ding, Nat. Phys. **11**, 724 (2015).

[13] H. Weng, C. Fang, Z. Fang, B. A. Bernevig, and X. Dai, Phys. Rev. X **5**, 011029 (2015).

[14] S.-Y. Xu, N. Alidoust, I. Belopolski, Z. Yuan, G. Bian, T.-R. Chang, H. Zheng, V. N. Strocov, D. S. Sanchez, G. Chang, C. Zhang, D. Mou, Y. Wu, L. Huang, C.-C. Lee, S.-M. Huang, B. Wang, A. Bansil, H.-T. Jeng, T. Neupert, A. Kaminski, H. Lin, S. Jia, and M. Zahid Hasan, Nat. Phys. **11**, 748 (2015).

[15] S.-Y. Xu, I. Belopolski, D. S. Sanchez, C. Zhang, G. Chang, C. Guo, G. Bian, Z. Yuan, H. Lu, T.-R. Chang, P. P. Shibayev, M. L. Prokopovych, N. Alidoust, H. Zheng, C.-C. Lee, S.-M. Huang, R. Sankar, F. Chou, C.-H. Hsu, H.-T. Jeng, A. Bansil, T. Neupert, V. N. Strocov, H. Lin, S. Jia, and M. Z. Hasan, Sci. Adv. **1**, e1501092 (2015).

[16] A. B. Sushkov, J. B. Hofmann, G. S. Jenkins, J. Ishikawa, S. Nakatsuji, S. Das Sarma, and H. D. Drew, Phys. Rev. B **92**, 241108(R) (2015).

[17] C. Shekhar, A. K. Nayak, Y. Sun, M. Schmidt, M. Nicklas, I. Leermakers, U. Zeitler, Y. Skourski, J. Wosnitza, Z. Liu, Y. Chen, W. Schnelle, H. Borrmann, Y. Grin, C. Felser, and B. Yan, Nat. Phys. **11**, 645 (2015).

[18] A. A. Soluyanov, D. Gresch, Z. Wang, Q. Wu, M. Troyer, X. Dai, and B. A. Bernevig, Nature (London) **527**, 495 (2015).

[19] C. Wang, Y. Zhang, J. Huang, S. Nie, G. Liu, A. Liang, Y. Zhang, B. Shen, J. Liu, C. Hu, Y. Ding, D. Liu, Y. Hu, S. He, L. Zhao, L. Yu, J. Hu, J. Wei, Z. Mao, Y. Shi, X. Jia, F. Zhang, S. Zhang, F. Yang, Z. Wang, Q. Peng, H. Weng, X. Dai, Z. Fang, Z. Xu, C. Chen, and X. J. Zhou, Phys. Rev. B **94**, 241119(R) (2016).

[20] B. Xu, Y. M. Dai, L. X. Zhao, K. Wang, R. Yang, W. Zhang, J. Y. Liu, H. Xiao, G. F. Chen, A. J. Taylor, D. A. Yarotski, R. P. Prasankumar, and X. G. Qiu, Phys. Rev. B **93**, 121110(R) (2016).

[21] A. Tamai, Q. S. Wu, I. Cucchi, F. Y. Bruno, S. Riccò, T. K. Kim, M. Hoesch, C. Barreteau, E. Giannini, C. Besnard, A. A. Soluyanov, and F. Baumberger, Phys. Rev. X **6**, 031021 (2016).

[22] L. Huang, T. M. McCormick, M. Ochi, Z. Zhao, M.-T. Suzuki, R. Arita, Y. Wu, D. Mou, H. Cao, J. Yan, N. Trivedi, and A. Kaminski, Nat. Mater. **15**, 1155 (2016).

[23] E. Liu, Y. Sun, N. Kumar, L. Muechler, A. Sun, L. Jiao, S.-Y. Yang, D. Liu, A. Liang, Q. Xu, J. Kroder, V. Süß, H. Borrmann, C. Shekhar, Z. Wang, C. Xi, W. Wang, W. Schnelle, S. Wirth, Y. Chen, S. T. B. Goennenwein, and C. Felser, Nat. Phys. **14**, 1125 (2018).

[24] Q. Xu, E. Liu, W. Shi, L. Muechler, J. Gayles, C. Felser, and Y. Sun, Phys. Rev. B **97**, 235416 (2018).

[25] Q. Wang, Y. Xu, R. Lou, Z. Liu, M. Li, Y. Huang, D. Shen, H. Weng, S. Wang, and H. Lei, Nat. Commun. **9**, 3681 (2018).

[26] H. B. Nielsen and M. Ninomiya, Phys. Lett. B **130**, 389 (1983).

[27] K. Nomura and N. Nagaosa, Phys. Rev. Lett. **106**, 166802 (2011).

[28] M. Z. Hasan and C. L. Kane, Rev. Mod. Phys. **82**, 3045 (2010).

[29] P. Hosur, Phys. Rev. B **86**, 195102 (2012).

[30] R. Okugawa and S. Murakami, Phys. Rev. B **89**, 235315 (2014).

[31] A. C. Potter, I. Kimchi, and A. Vishwanath, Nat. Commun. **5**, 5161 (2014).

[32] Y. Sun, S.-C. Wu, and B. Yan, Phys. Rev. B **92**, 115428 (2015).

[33] C.-C. Lee, S.-Y. Xu, S.-M. Huang, D. S. Sanchez, I. Belopolski, G. Chang, G. Bian, N. Alidoust, H. Zheng, M. Neupane, B. Wang, A. Bansil, M. Z. Hasan, and H. Lin, Phys. Rev. B **92**, 235104 (2015).

[34] V. Aji, Phys. Rev. B **85**, 241101(R) (2012).

[35] D. T. Son and B. Z. Spivak, Phys. Rev. B **88**, 104412 (2013).

[36] A. A. Burkov, Phys. Rev. Lett. **113**, 187202 (2014).

[37] S. A. Parameswaran, T. Grover, D. A. Abanin, D. A. Pesin, and A. Vishwanath, Phys. Rev. X **4**, 031035 (2014).

[38] A. A. Burkov, J. Phys.: Condens. Matter. **27**, 1 (2015).

[39] Y. Baum, E. Berg, S. A. Parameswaran, and A. Stern, Phys. Rev. X **5**, 041046 (2015).

[40] X. Huang, L. Zhao, Y. Long, P. Wang, D. Chen, Z. Yang, H. Liang, M. Xue, H. Weng, Z. Fang, X. Dai, and G. Chen, Phys. Rev. X **5**, 031023 (2015).

[41] C.-L. Zhang, S.-Y. Xu, I. Belopolski, Z. Yuan, Z. Lin, B. Tong, G. Bian, N. Alidoust, C.-C. Lee, S.-M. Huang, T.-R. Chang, G. Chang, C.-H. Hsu, H.-T. Jeng, M. Neupane, D. S. Sanchez, H. Zheng, J. Wang, H. Lin, C. Zhang, H.-Z. Lu, S.-Q. Shen, T. Neupert, M. Zahid Hasan, and S. Jia, Nat. Commun. **7**, 10735 (2016).

[42] B. Z. Spivak and A. V. Andreev, Phys. Rev. B **93**, 085107 (2016).

[43] A. A. Zyuzin and R. P. Tiwari, JETP Lett. **103**, 717 (2016).

[44] F. Wilczek, Phys. Rev. Lett. **58**, 1799 (1987).

[45] P. E. C. Ashby and J. P. Carbotte, Phys. Rev. B **89**, 245121 (2014).

[46] P. Hosur and X.-L. Qi, Phys. Rev. B **91**, 081106(R) (2015).

[47] P. Goswami, G. Sharma, and S. Tewari, Phys. Rev. B **92**, 161110(R) (2015).

[48] J. Ma and D. A. Pesin, Phys. Rev. B **92**, 235205 (2015).

[49] M. Kargarian, M. Randeria, and N. Trivedi, Sci. Rep. **5**, 3045 (2015).

[50] K. Taguchi, T. Imaeda, M. Sato, and Y. Tanaka, Phys. Rev. B **93**, 201202(R) (2016).

[51] J. Hofmann and S. Das Sarma, Phys. Rev. B **93**, 241402(R) (2016).

[52] C.-K. Chan, N. H. Lindner, G. Refael, and P. A. Lee, Phys. Rev. B **95**, 041104(R) (2017).

[53] K. Halterman, M. Alidoust, and A. Zyuzin, Phys. Rev. B **98**, 085109 (2018).

[54] A. A. Zyuzin and A. A. Burkov, Phys. Rev. B **86**, 115133 (2012).

[55] M. M. Vazifeh and M. Franz, Phys. Rev. Lett. **111**, 027201 (2013).

[56] E. Barnes, J. J. Heremans, and D. Minic, Phys. Rev. Lett. **117**, 217204 (2016).

[57] F. M. D. Pellegrino, M. I. Katsnelson, and M. Polini, Phys. Rev. B **92**, 201407(R) (2015).
[58] Y. Ferreirós and A. Cortijo, Phys. Rev. B **93**, 195154 (2016).
[59] Q. Li, D. E. Kharzeev, C. Zhang, Y. Huang, I. Pletikosic, A. V. Fedorov, R. D. Zhong, J. A. Schneeloch, G. D. Gu, and T. Valla, Nat. Phys. **12**, 550 (2016).
[60] P. Baireuther, J. A. Hutasoit, J. Tworzydło, and C. W. J. Beenakker, New J. Phys. **18**, 045009 (2016).
[61] B. Rosenstein, H. C. Kao, and M. Lewkowicz, Phys. Rev. B **95**, 085148 (2017).
[62] M. S. Ukhtary, A. R. T. Nugraha, and R. Saito, J. Phys. Soc. Jpn. **86**, 104703 (2017).
[63] J. Zhou and H.-R. Chang, Phys. Rev. B **97**, 075202 (2018).
[64] O. V. Kotov and Y. E. Lozovik, Phys. Rev. B **98**, 195446 (2018).
[65] T. Tamaya, T. Kato, K. Tsuchikawa, S. Konabe, and S. Kawabata, J. Phys.: Condens. Matter **31**, 305001 (2019).
[66] I. Panfilov, A. A. Burkov, and D. A. Pesin, Phys. Rev. B **89**, 245103 (2014).
[67] J. Zhou, H.-R. Chang, and D. Xiao, Phys. Rev. B **91**, 035114 (2015).
[68] J. Hofmann and S. Das Sarma, Phys. Rev. B **91**, 241108(R) (2015).
[69] J. C. W. Song and M. S. Rudner, Phys. Rev. B **96**, 205443 (2017).
[70] P. Goswami and S. Tewari, Phys. Rev. B **88**, 245107 (2013).
[71] J. Tominaga, A. V. Kolobov, P. Fons, T. Nakano, and S. Murakami, Adv. Mater. Interfaces **1**, 1300027 (2013).
[72] R. F. Wallis, J. J. Brion, E. Burstein, and A. Hartstein, Phys. Rev. B **9**, 3424 (1974).
[73] E. V. Gorbar, V. A. Miransky, I. A. Shovkovy, and P. O. Sukhachov, Phys. Rev. B **99**, 155120 (2019).
[74] G. M. Andolina, F. M. D. Pellegrino, F. H. L. Koppens, and M. Polini, Phys. Rev. B **97**, 125431 (2018).
[75] Q. Chen, A. R. Kutayiah, I. Oladyshkin, M. Tokman, and A. Belyanin, Phys. Rev. B **99**, 075137 (2019).
[76] P. G. Flahive and J. J. Quinn, Phys. Rev. Lett. **31**, 586 (1973).
[77] C. Uberoi and U. J. Rao, Solid State Commun. **21**, 579 (1977).
[78] U. J. Rao and C. Uberoi, Phys. Rev. B **18**, 2941 (1978).
[79] P. Halevi and J. J. Quinn, Solid State Commun. **33**, 467 (1980).
[80] K. S. Yi, J. J. Quinn, and P. Halevi, Phys. Rev. B **22**, 6247 (1980).
[81] S. T. Ivanov and N. I. Nikolaev, J. Phys. D: Appl. Phys. **29**, 1107 (1996).
[82] S. T. Ivanov, N. I. Nikolaev, and R. W. Thomae, Phys. Scr. **57**, 645 (1998).